Available online at www.sciencedirect.com
ScienceDirect
Proceedings of the Combustion Institute 000 (2022) 1–10
Proceedings of the Combustion Institute
www.elsevier.com/locate/proci

On polyhedral structures of lean methane/hydrogen Bunsen flames: Combined experimental and numerical analysis

Haris Lulic [a,1], Adrian Breicher [b,c,1], Arne Scholtissek [a,*], Pasquale Eduardo Lapenna [d], Andreas Dreizler [c], Francesco Creta [d], Christian Hasse [a], Dirk Geyer [b], Federica Ferraro [a]

[a] *Technical University of Darmstadt, Department of Mechanical Engineering, Simulation of reactive Thermo-Fluid Systems, Otto-Berndt-Str. 2, 64287 Darmstadt, Germany*
[b] *Darmstadt University of Applied Sciences, Laboratory for Optical Diagnostics and Renewable Energies, Schoefferstr. 3, 64295 Darmstadt, Germany*
[c] *Technical University of Darmstadt, Department of Mechanical Engineering, Reactive Flows and Diagnostics, Otto-Berndt-Str. 3, 64287 Darmstadt, Germany*
[d] *Department of Mechanical and Aerospace Engineering, Sapienza University of Rome, via Eudossiana 18, 00184 Rome, Italy*

Received 5 January 2022; accepted 19 July 2022
Available online xxx

Abstract

In premixed flame propagation of lean hydrogen or hydrogen-enriched blends, both hydrodynamic and thermo-diffusive instabilities are governing the flame front shape and affect its propagation velocity. As a result, different types of cellular patterns can occur along the flame front in a laminar scenario. In this context, an interesting phenomenon is the formation of polyhedral flames which can be observed in a Bunsen burner. It is the objective of this work to systematically characterize the polyhedral structures of premixed methane/hydrogen Bunsen flames in a combined experimental and numerical study. A series of lean flames with hydrogen content varying between 20 and 85% at two equivalence ratios is investigated. The experiments encompass chemiluminescence imaging together with Planar Laser-induced Fluorescence (PLIF) measurements of the OH radical. Characteristic cell sizes are quantified from the experiments and related to the characteristic length scales obtained from a linear stability analysis. In the experiments, it is observed that the cell sizes at the base of the polyhedral Bunsen flames decrease almost linearly with hydrogen addition and only a weak dependence on the equivalence ratio is noted. These trends are well reflected in the numerical results and the length scale comparison further shows that the wavelength with the maximum growth rate

* Corresponding author.
E-mail address: scholtissek@stfs.tu-darmstadt.de (A. Scholtissek).
[1] Joint First Authors.

https://doi.org/10.1016/j.proci.2022.07.251

Please cite this article as: H. Lulic, A. Breicher, A. Scholtissek et al., On polyhedral structures of lean methane/hydrogen Bunsen flames: Combined experimental and numerical analysis, Proceedings of the Combustion Institute, https://doi.org/10.1016/j.proci.2022.07.251

predicted by the linear stability analysis is comparable to the cell size obtained from the experiment. The correlation between the experimental findings and the linear stability analysis is discussed from multiple perspectives considering the governing time and length scales, furthermore drawing relations to previous studies on cellular flames.

Keywords: Cellular structures; Intrinsic instabilities; Linear stability analysis; Hydrogen enriched fuel blends; Polyhedral flames,

1. Introduction

In premixed flame propagation, often intrinsic instabilities are governing the flame front shape and its propagation velocity, even in the case without surrounding elements interacting with the flame [1]. Intrinsic flame front instabilities can generally be described in terms of two main mechanisms: hydrodynamic or Darrieus-Landau (DL) and thermo-diffusive (TD) instabilities [2]. Hydrodynamic instabilities are caused by thermal expansion of the fluid approaching the flame front and have a destabilizing effect for any perturbation, assuming an infinitely thin flame, while thermo-diffusive effects can be stabilizing or destabilizing depending on the effective Lewis number of the mixture [3], when analysing a curved flame front in general. Both, DL and TD instabilities, are expected to be present in case of lean hydrogen or hydrogen-enriched fuel blends.

The combined effect of these intrinsic instabilities can manifest itself in different ways and it highly depends on the flame configuration, since also type and size of the confinement of the flame [2,4] and the interaction of the flame with the burner play a role. In practical scenarios, the onset of instabilities is related to an initial perturbation that causes the destabilization of the flame front. Such perturbations are characterized by their wavelength, a characteristic length scale of the perturbation. As discussed by Creta et al. [2] there exists a critical wavelength λ_c, a mixture-dependent length scale larger than the flame thickness [4], regardless of the stabilizing or destabilizing effect of the TD instabilities. If the initial perturbation wavelength exceeds this critical value, the flame is destabilized. Flame instabilities develop if the characteristic hydrodynamic length scale L constraining the flame (e.g. the characteristic dimension of the burner nozzle or the domain width for a flame propagating in a channel) is higher than the critical wavelength [2]. In this case, the formation of cellular structures along the flame front can be observed. Even in the case of weakly turbulent induced instabilities, large scale effects due to intrinsic instabilities are important in the flames constrained by a domain size $L > \lambda_c$ and they can in general be classified as large scale flames [4]. Comprehensive studies on stability and structure of cellular flames with a wide range of experimental data can be found in [5].

Polyhedral flames, a variant of cellular flames [5], can be observed in the Bunsen flame configuration in case the deficient reactant is also the lighter one [6]. Polyhedral flames were firstly observed by Smithells and Ingle [7] and studied in detail for the first time by Smith and Pickering [8]. The authors found that the number of corrugations of polyhedral Bunsen flames is a function of the size of the burner tube and the fresh gas mixture composition [8]. Later, Sohrab and Law [9] studied the characteristics of propane and butane polyhedral flames. They found that the number of corrugations varies with the flow velocity and the mixture composition. Stable and rotating polyhedral flames were categorized by means of a stability diagram and a varying number of cusps was identified for a range of compositions and velocities. Two peculiar characteristics of polyhedral flames are the rotation of the unstable structures [8] and the appearance of secondary cellular structures [10]. Rotation can originate from a change of composition and it is related to the tendency of the flame to shift between two stable conditions with a different number of corrugations [8]. In these first studies, attempts have been made to characterize the cell sizes. Markstein [5] discussed the importance of a critical wavelength and proposed to relate the minimum rather than the average cell size to the critical wavelength. Jacobi and Sohrab [10] underlined the importance of thermo-diffusive length scales and related them to the cell size.

The earliest indications of the relation of the most unstable wavelength and the cell size in planar/spherical flames are found in the theoretical work of Sivashinsky [11]. Recently, efforts have been made to characterize the cell size (the range of instability wavelengths) of unstable flame fronts in planar [12–15] and circular expanding [16] flames. Kadowaki and Hasegawa [13] studied intrinsic instabilities by means of 2D and 3D linear stability analysis (LSA). The resulting dispersion relations from the 2D and the 3D cases were found comparable. Numerical simulations of unconfined planar flames with large computational domains have also been performed. In such cases, the observed aver-

Please cite this article as: H. Lulic, A. Breicher, A. Scholtissek et al., On polyhedral structures of lean methane/hydrogen Bunsen flames: Combined experimental and numerical analysis, Proceedings of the Combustion Institute, https://doi.org/10.1016/j.proci.2022.07.251

No. of cells	8	11	12(13)	14(15)	15	16	13(12)	15(14)	15	16(17)	18(19)	19(20)	21
H_2Vol. − %	20	40	50	60	65	70	50	60	65	70	75	80	85
ϕ	0.80	0.80	0.80	0.80	0.80	0.80	0.65	0.65	0.65	0.65	0.65	0.65	0.65
u_{bulk}[m/s]	0.80	1.20	1.50	2.00	2.20	2.35	1.30	1.70	1.75	1.90	2.05	2.30	2.60
α	40°	40°	40°	30°	30°	30°	30°	30°	30°	30°	30°	30°	40°

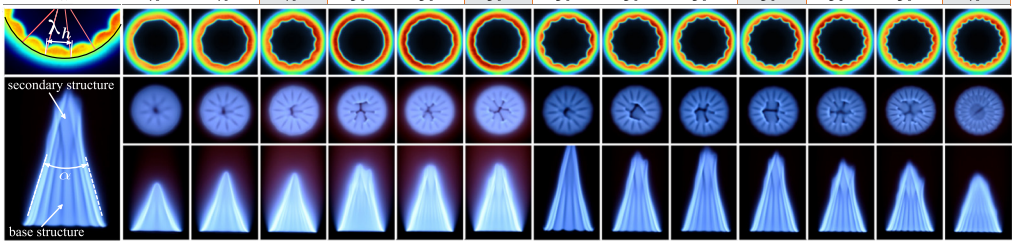

Fig. 1. Top view OH − PLIF at 2mm axial height (top) as well as chemiluminescence images of the top view (middle) and side view (bottom) of the polyhedral Bunsen flames. Flames are ordered according to the increasing number of cells and H_2 content. The volumetric hydrogen content of the CH_4/H_2 mixtures is given by H_2 Vol.-%, equivalence ratio by ϕ and flame cone angle by α. u_{bulk} is the bulk flow velocity. OH-PLIF images show the flame realizations with the number of cells that were most likely to occur. Values in brackets denote the number of cells observed in the experiment by OH PLIF with lower likelihood.

age cell size has been shown to be slightly larger than the most unstable wavelength [12]. Altantzis et al. [15] investigated the development of instabilities in two-dimensional lean hydrogen planar flames. The authors studied the linear growth and nonlinear evolution of the instabilities for different domain heights. For larger domain heights (20–80 thermal flame thicknesses), dominant single cusp structures have been observed with the wavelengths comparable to the domain height. Cells that are formed after the initial perturbation and cells that are later continuously formed along the low curvature sides of the cusp had sizes corresponding to the wavelength with the highest growth rate [15]. Berger et al. [14] performed detailed numerical simulations of unconfined, large scale, lean hydrogen planar flames and statistically characterized the cell size. The existence of the smallest and the largest intrinsic length scales was shown and the authors suggested that the smallest length scale corresponds to the most unstable wavelength predicted by their linear stability analysis. A relation of the most unstable wavelength from the dispersion relation and flame propagation velocity can also be made in turbulent flows [17].

Similar analyses, which focus on the cell sizes of polyhedral Bunsen flames, are rarely found in the literature. It is the objective of this paper to systematically characterise the polyhedral structures of lean premixed methane/hydrogen Bunsen flames in a combined experimental and numerical study. Characteristic cell sizes observed in the experiments are quantified and related to characteristic length scales obtained from a linear stability analysis. The study is performed for hydrogen contents varying from 20 to 85 Vol.-% (≡ % H_2 in the following) considering two equivalence ratios (0.8 and 0.65). An overview of the flames analyzed in this study

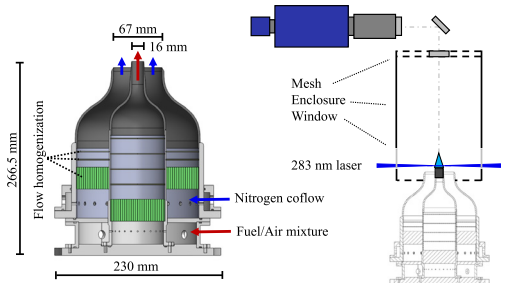

Fig. 2. Schematic of the laminar jet burner including the diagnostics.

with their peculiar polyhedral structure can be seen in Fig. 1.

2. Experimental measurements

2.1. Experimental setup

The flames were stabilized on a laminar jet burner consisting of a central jet (exit diameter 16 mm) and a surrounding co-flow (exit diameter 67 mm). Figure 2 shows the burner schematically, including the contoured contractions used to create block-shaped flow profiles at the exit of the central jet and the co-flow. The jet nozzle ended in a straight tube with a length of 31.5 mm. A tube wall thickness of 0.5 mm ensured that bluff body effects were minimized. Within the burner, several stages of screens and honeycombs were arranged to homogenize the main and co-flow before entering the contoured nozzle geometries, where the central jet contour had a contraction ratio of 20.25. An en-

Please cite this article as: H. Lulic, A. Breicher, A. Scholtissek et al., On polyhedral structures of lean methane/hydrogen Bunsen flames: Combined experimental and numerical analysis, Proceedings of the Combustion Institute, https://doi.org/10.1016/j.proci.2022.07.251

closure with a width of 15 jet diameters was used to protect the flames from environmental influences while windows on the sides and top allowed access for optical measurement systems. Screens over the entire area of the inlet and outlet section ensured that atmospheric pressure prevailed in the enclosure.

Mass flow controllers (Bronkhorst, EL-FLOW, maximum deviation of 0.85%) were used to meter the flow rates of the CH_4/H_2/air flow composition in the central jet. N_2 was used as gas in the co-flow. To obtain a constant flame cone angle (30° or 40°), the bulk velocity of the central jet was increased accordingly with increasing hydrogen content. The lower flanks of the flame have been used as the reference for determining the angle due to occasional flame flickering close to the flame tip (see Fig. 1).

To quantify the number of cells and the corrugated flame front shape Planar Laser-induced Fluorescence (PLIF) measurements of the OH radical was used to capture horizontal cross-sections of the flame cone at an axial height of 2 mm. A frequency-doubled Nd:YAG laser (Spitlight 1000.2, Innolas, 10 Hz repetition rate) pumped a dye laser (Cobra-Stretch, Sirah) with Rodamine 6G and another frequency doubler to form a light sheet at 283 nm (0.15 cm^{-1} spectral width, 1.4 mJ). The light sheet of 25 mm width was focused into a thickness of 110 μm within the probe volume. The fluorescence of OH radical was imaged by a bandpass filter (315 nm, ±15) and a 105 mm UV objective onto an image intensifier (IRO X, LaVision) and a CMOS camera (Imager M-Lite, LaVision) resulting in a resolution of 125 μm. Chemiluminescence images of the flames were taken to capture the overall structure of the flame from a side and top view.

The main focus of this study is put on the primary cellular structures at the flame base. The cells are initially formed along the circumference, and once formed, are convected upwards along the flame cone. Additionally, non-linear effects, such as cell merging, can play a role. Therefore, the circumference of the burner is selected as a hydrodynamic length which is independent from the inlet velocity and common to all studied flames. Accordingly, the average cell size was determined at the burner rim. It is noted, that the cell size is smaller at higher heights for a fixed number of cells, but the selection of some other height, e.g. 2 mm, would be arbitrary and would introduce inconsistencies in terms of different additional convective time between the cases and different local mixture composition, which can occur due to preferential diffusion along the Bunsen cone [18,19]. Figure 1 shows that the cells are regularly distributed around the circumference. Hence, the cell size can be consistently determined dividing the circumference of the burner by the number of cells (λ_h in Fig. 1).

2.2. Phenomenological observations

Figure 1 depicts the OH-PLIF and chemiluminescence images of the flames, with information about the number of cells observed, hydrogen content, equivalence ratio, and cone angle. Some cases, mainly the leaner ones at $\phi = 0.65$, stabilized with varying numbers of cells. Flames with a number of cells, which were less likely to occur in the experiment, are shown with the chemiluminescence images, and the number is indicated in brackets on Fig. 1. The OH-PLIF images show the number of cells that were most likely to occur.

For mixtures with lower hydrogen content (20-50% H_2), with $\phi = 0.8$ and cone angle $\alpha = 40°$, a weaker cellular structure was found that is strengthened with increasing hydrogen content (see Fig. 1). It was enhanced mainly in the middle cone region for lower hydrogen contents. When these flames were stabilised with $\alpha = 30°$, the cellular structures were suppressed by the increased inlet velocity, and only for 40 and 50% H_2 weak cellular patterns were observed near the flame tip (not shown). In these two cases, the same number of cells was present as for the 40° cone angle. For mixtures with 50 to 85% H_2, at $\phi = 0.65$, distinct cellular structures starting from the flame leading edge were observed. Flames were stabilized with $\alpha = 30°$, except for the 85% H_2 case, where $\alpha = 40°$. This regular structure is maintained to the flame tip, where secondary cellular structures became prevalent. The size of the secondary structure tends to moderately increase with hydrogen addition, as can be seen from the top view images. The cases with 60, 65, and 70% H_2 were also measured with $\phi = 0.8$ and $\alpha = 30°$ and the number of cells showed almost no change. For the 60% H_2 – ϕ0.8 case, the primary structure is the weakest and located mainly in the upper cone region.

For both equivalence ratios investigated, a clear dependence of the cell size (number of cells) on the hydrogen content is found. The cell size decreases almost linearly with the hydrogen addition. On the other hand, a weak dependence of the cell size to the equivalence ratio is noted, while the onset of instabilities is moderately shifted up in the axial direction with the higher equivalence ratio. Moreover, it is observed that the depth of the cell ridges is affected by the equivalence ratio. Specifically, the instability amplitude appears larger for lower equivalence ratio (see Fig. 1).

3. Linear stability analysis

A numerical linear stability analysis (LSA) has proven to be a powerful technique for studying flame instabilities [12,15,20,21]. Although in the non-linear regime of propagation, the characteristic dimensions of the corrugations will differ from those obtained from LSA, the latter remains a rigorous measure of the flame tendency to develop

Please cite this article as: H. Lulic, A. Breicher, A. Scholtissek et al., On polyhedral structures of lean methane/hydrogen Bunsen flames: Combined experimental and numerical analysis, Proceedings of the Combustion Institute, https://doi.org/10.1016/j.proci.2022.07.251

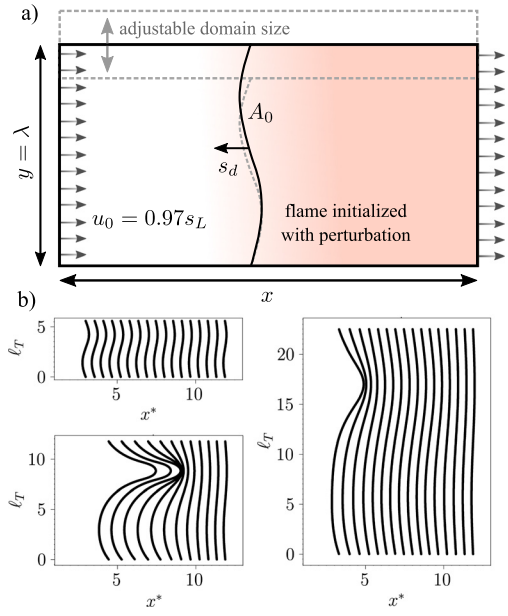

Fig. 3. Schematic of the computational domain with a perturbed planar flame (a) and exemplary evolutions of the inner layer temperature isolines shown for the case 70% H_2 – ϕ0.80 and different domain heights (λ = 5.6, 11.75 and 22.50ℓ_T) (b). The isolines extracted every Δt = 0.5 ms are shifted for visual inspection using the following transformation $x^{t+\Delta t} = x^t - \Delta t \cdot 10^3$ leading to a modified spatial coordinate x^*.

corrugations. In this work, a LSA of planar flames, whose initial conditions are comparable to the experiments, is performed using direct numerical simulations to obtain the range of unstable wavelengths and the corresponding growth rates in the form of dispersion relations. The resulting length and time scales are subsequently analyzed in terms of their relationship to the character and range of instabilities found in the experiments. For details on the dispersion relation readers are referred to [1,2,15] and comparisons of LSA to experiments can be found in [5,22,23]. The canonical planar flame configuration has been chosen for LSA in several previous works and it has been shown that it can provide insights into the instability characteristics of more complex experimental or numerical flame configurations (see, e.g. [4,24–26]).

Planar flames (Fig. 3a) are initialized with a small sinusoidal perturbation ($A_0 = 0.04\,\ell_T$, with the thermal flame thickness $\ell_T = (T_b - T_u)/\max(dT/dx)$) of wavelength λ which corresponds to the domain size in the lateral direction y. The growth rate of the perturbation $\omega = d(\ln A(t)/A_0)/dt$ is calculated tracking the amplitude of the inner layer temperature isoline versus time. Three exemplary evolutions of the flame front are illustrated in Fig. 3b for one mixture with different initial perturbations.

Simulations are performed with a reactive flow solver based on OpenFOAM (v2006) [27] utilizing a skeletal reaction mechanism [28] developed for atmospheric CH_4/H_2/air combustion and a mixture average transport model [29]. The transport properties are obtained from the EGLib transport library [30]. The Soret and Dufour effects are neglected. All flames are initialised with 1D flame profiles and displaced in the lateral direction to reflect the initial perturbation (Fig. 3a). A uniform velocity profile is prescribed at the inlet, which is chosen slightly lower than the unstretched laminar burning velocity in order to enable a slow flame propagation. The domain size in the longitudinal direction x is kept constant and is large enough to allow for an unconstrained flame propagation and instability evolution. In the lateral direction periodic boundary conditions are used. The thermal flame thickness is resolved with 40 points in a uniform computational grid in both directions. Based on previous works, e.g., [14,31,32], it can be concluded that this resolution is suitable to resolve the unstable flame front. A grid independence study further showed for the 40% H_2 blend with $\phi = 0.8$ that a flame front resolution between 30 and 40 grid points results in less than 3% deviation for all growth rates. The discretization schemes are 2^{nd} order in space and 1^{st} order in time with the Courant number set to 0.1.

The dispersion relation is then obtained in the form $\omega = \omega(k)$, where k is the wavenumber of the perturbation $k = 2\pi/\lambda$. The dispersion relation yields the range of unstable (and stable) wavenumbers, the critical (neutral) wavelength $\lambda_c = 2\pi/k_c$ at which the transition from negative to positive growth rate occurs, and the most unstable wavelength $\lambda(\omega_{\max}) = 2\pi/k(\omega_{\max})$ corresponding to the maximum growth rate $\omega_{\max}$. k_c is the critical (neutral) wavenumber. In this form, the dispersion relation accounts for both DL and TD instabilities for a given initial thermochemical state of the fresh gas mixture defined by temperature T, pressure p, and equivalence ratio ϕ as well as hydrogen content. The dispersion relations are fitted with a polynomial considering 1st, 2nd, and 4th order terms. The appropriateness and necessity of using such a fitting function for mixtures with low Le_{eff} are discussed in further detail in [2,15].

4. Correlation between experiments and linear stability analysis

The LSA is performed for a subset of the experimental cases listed in Table 1, along with the important unstretched flame characteristics. The numerical dataset reflects the wide range of hydrogen content and the range of equivalence ratios considered in the experiments. First, the effect of hydro-

Please cite this article as: H. Lulic, A. Breicher, A. Scholtissek et al., On polyhedral structures of lean methane/hydrogen Bunsen flames: Combined experimental and numerical analysis, Proceedings of the Combustion Institute, https://doi.org/10.1016/j.proci.2022.07.251

Table 1
Fresh gas mixtures and conditions considered in the LSA, with characteristics of the unstretched premixed flames. s_L and T_b are the laminar burning velocity and the maximum flame temperature, respectively. For each mixture, the effective Lewis number $\mathrm{Le_{eff}}$, the expansion ratio σ and the Zeldovich number β are given.

% H_2 − ϕ − T_0	s_L[m/s]	T_b[K]	ℓ_T[mm]	$\mathrm{Le_{eff}}$	σ	β
50 − 0.80 − 300 K	0.426	2039.2	0.4026	0.859	6.60	8.54
70 − 0.80 − 300 K	0.619	2067.8	0.3441	0.814	6.54	8.06
70 − 0.65 − 300 K	0.387	1823.9	0.4320	0.714	5.82	8.78
85 − 0.65 − 300 K	0.609	1860.3	0.3717	0.664	5.79	7.98

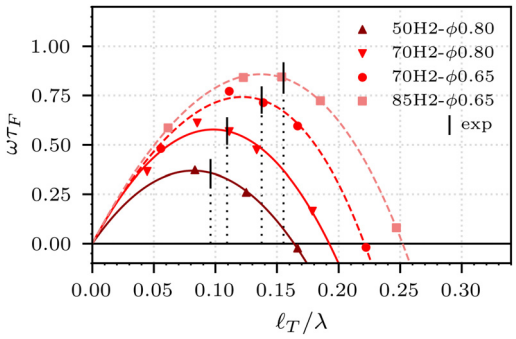

Fig. 4. Dispersion relations for methane/hydrogen mixtures calculated for $T_0 = 300$ K. Each point corresponds to one numerical simulation with a different domain size $y = \lambda$. The continuous lines are 4th order polynomials.

gen addition is analyzed, then the variation of the equivalence ratio is investigated considering both numerical and experimental results.

4.1. Variation of hydrogen content

The dispersion relations obtained for mixtures with different hydrogen content and an initial temperature $T_0 = 300$ K (see Table 1) are depicted in Fig. 4. The wavelength is normalised by the ℓ_T, while the flame time $\tau_F = \ell_T / s_L$ is used to normalise the growth rate. The cell sizes estimated from experiments are marked on Fig. 4 for each mixture along with the corresponding dispersion relation. They are normalised accordingly with ℓ_T and indicated by black vertical lines. For every mixture, the wavelength (cell size - λ_h) of the observed instabilities in the experiment agrees reasonably well with the most unstable wavelength $\lambda(\omega_{\max})$, which is determined from the dispersion relation. This is also shown quantitatively in Table 2 where several relevant parameters from the experiment and the LSA are listed. This correlation implies that the dispersion relation of planar flames and the corresponding location of the highest growth rate can be used to approximate the number of cells in the polyhedral Bunsen flames. However, it is observed that λ_h is slightly shifted towards $\lambda < \lambda(\omega_{\max})$ in all cases (see Table 2), and 1–3 less cells would be predicted using $\lambda(\omega_{\max})$.

The dispersion relations shown in Fig. 4 include two hydrogen blending levels for each equivalence ratio considered. The average cell size (λ_h in Table 2) decreases with hydrogen addition in both cases. From the dispersion relations in Fig. 4, it is observed that an increasing hydrogen content leads to a wider range of instability modes, a decrease of the wavelength with maximum growth rate $\lambda(\omega_{\max})$ and an increase in the normalised growth rate. The wider range of instability modes (lower value of the critical wavelength λ_c) implies the possibility of formation of smaller cells, while the shift in $\lambda(\omega_{\max})$ implies a decreasing size of the fastest growing cells. Different $\lambda(\omega_{\max})$ result in a different average cell size in fully developed unstable flames [14] and a higher normalised growth rate would cause enhanced cellular structures and deeper cusps of the cells.

If the most unstable wavelengths extracted from the dispersion relation (see Table 2) are directly compared to the cell size, differences of 11–17% are found. This represents a reasonable agreement, considering the complexity of the configuration and that the compressed nature of the Bunsen burner could modify the stability properties compared to the planar flame configuration. Furthermore, the trend of change of the peak position $\lambda(\omega_{\max})$ in the dispersion relation is similar, ∼29% and ∼23% decrease, as for the measured cell size, ∼25 and ∼24% decrease, for lower and higher equivalence ratio, respectively.

The increase of the maximum growth rate with H_2 addition is also in agreement with the strengthening of the cellular structure observed in experiments.

4.2. Variation of equivalence ratio

Mixtures with 50, 60, 65 and 70% H_2 are measured at two equivalence ratios, $\phi = 0.65$ and 0.8 (see Fig. 1). An interesting observation from the experiments is that the number of cells is weakly affected by the equivalence ratio. It remains unchanged or increases/decreases by one. Further, the main differences between higher and lower equivalence ratio cases are the deeper negatively curved parts in the main cone zone for the latter case. The LSA is performed for the 70% H_2 case for both equivalence ratios in Fig. 4. 16 cells are observed

Please cite this article as: H. Lulic, A. Breicher, A. Scholtissek et al., On polyhedral structures of lean methane/hydrogen Bunsen flames: Combined experimental and numerical analysis, Proceedings of the Combustion Institute, https://doi.org/10.1016/j.proci.2022.07.251

Table 2
Comparison of relevant parameters from the experiment and from the LSA. The estimated cell size at the flame base is given by λ_h, while the residence time, $t_{res} = H/u_{bulk}$, is computed based on the flame height H determined from the burner diameter D and the cone angle α. $\lambda(\omega_{max})$ is the most unstable wavelength determined from the dispersion relation, and the time scale corresponding to the maximum growth rate is computed as $t_{inst} = 1/\omega_{max}$.

	experiment		LSA	
% H_2 – ϕ – T_0	λ_h[mm]	t_{res}[ms]	$\lambda(\omega_{max})$[mm]	$t_{inst}(1/\omega_{max})$[ms]
50 – 0.80 – 300 K	4.19 ($\sim 10.40\ell_T$)	14.65	4.92	2.56
70 – 0.80 – 300 K	3.14 ($\sim 9.13\ell_T$)	12.70	3.50	0.96
70 – 0.65 – 300 K	3.14 ($\sim 7.27\ell_T$)	17.56	3.55	1.50
85 – 0.65 – 300 K	2.39 ($\sim 6.44\ell_T$)	11.48	2.72	0.71

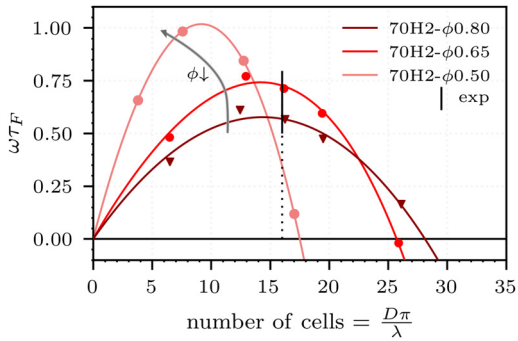

Fig. 5. Dispersion relations for 70% H_2 mixture with equivalence ratio variation shown on modified abscissa where the wavelength is normalised with the characteristic dimension of the burner $D\pi$. The abscissa represents the number of cells.

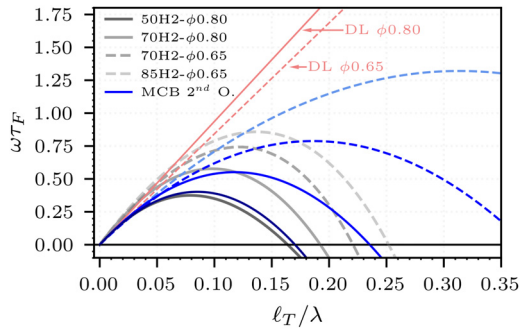

Fig. 6. Comparison of the numerical (grey) dispersion relations with the theoretical 2^{nd} order (MCB) expression (blue). The theoretical DL instability is shown in red. (For interpretation of the references to colour in this figure legend, the reader is referred to the web version of this article.)

in both cases (Fig. 1), and while the absolute cell size is not changed, the relative cell size (λ_h/ℓ_T) in Fig. 4 is different. This is caused by the change in the ℓ_T, which is ~25% larger for lower equivalence ratio.

From Fig. 4, it can be seen that the trend of change of peak position and experimental points are in agreement. This consistency is shown more intuitively, if the λ is normalised with the characteristic burner length. Thus, Fig. 5 shows the dispersion relations where λ is normalised with the burner circumference $D\pi$ and the abscissa directly represents the number of cells. By visual inspection of Fig. 5, the following conclusions can be drawn: the position of the peak of the dispersion relation related to $\lambda(\omega_{max})$ is not influenced significantly by the change of the equivalence ratio from the experiment (also visible in Tab. 2), while the critical wavelength λ_c changes. This weak dependency of the most unstable wavelength to the equivalence ratio explains why the number of cells observed in the experiments is not very sensitive to equivalence ratio changes. The difference in the unstretched flame thickness compensates for the shift of the two corresponding dispersion relations on Fig. 4. Illustrating the sensitivity with respect to ϕ, an additional dispersion relation closer to the lean limit ($\phi = 0.5$) is calculated. Based on the numerical results, a non-linear increase of λ_h is expected as the lean limit is approached (Fig. 5). This can be attributed to a non-linear increase of ℓ_T (~70% for $\phi_{0.65\rightarrow0.50}$ (c.f. supplementary material). In addition to the shift in critical wavelength λ_c, the normalised growth rate (the ordinate on Fig. 5) is increased by 15% with the decrease in the equivalence ratio considered in the experiment, while the increase for the additional leaner case is 37%. Since this represents the ratio of the flame time to the instability time scale, its increase promotes the instability and explains deeper negatively curved parts of cells for the lower equivalence ratio (see Fig. 1).

4.3. Comparison to theory

Next, the dispersion relations are compared to a theoretical relation by Matalon et al. [3] (MCB), which accounts for the diffusive transport in addition to the DL mechanism [1] (the mathematical expression is given in the supplementary material).

Theoretical dispersion relations are depicted in Fig. 6, along with the theoretical DL instability and the numerically determined relations shown in the background. There is a very good agreement for the 50% H_2 – ϕ0.8 case, while the numerical and the-

Please cite this article as: H. Lulic, A. Breicher, A. Scholtissek et al., On polyhedral structures of lean methane/hydrogen Bunsen flames: Combined experimental and numerical analysis, Proceedings of the Combustion Institute, https://doi.org/10.1016/j.proci.2022.07.251

oretical results start to deviate in the case of hydrogen addition (70% H_2 – ϕ0.8) with more significant deviations for the lower equivalence ratio, $\phi = 0.65$. In general, trends of the maximum growth rates and critical wavelengths are qualitatively in agreement, but they are overestimated quantitatively for the considered parameter variation. DL growth rates distinguish between two equivalence ratios only, since they are negligibly affected by the H_2 content. It can therefore be argued that the H_2 addition is mainly causing a shift in the TD mechanism. On the other hand, the equivalence ratio reduction is lowering the growth rates of the DL mechanism, while the trend of increased growth rates is governed by the TD mechanism. In general, the magnitudes of the DL growth rates indicate a significant contribution of the DL mechanism to the overall dispersion relation.

Further theoretical results based on the work of Sivashinsky [33] are presented in the supplementary material. The dispersion relations calculated with the Sivashinsky implicit relation can only be interpreted in terms of stabilising/destabilising contributions for the thermo-diffusive effect since the thermal expansion is not accounted for. The trend of change of the growth rates is qualitatively in agreement with the numerical results and the MCB expression.

4.4. Discussion

As previously shown, the instability modes obtained from the dispersion relation correlate well with the cellular structures observed in the experiments. Considering that the *transient evolution of an instability*, as obtained from the LSA, can be used to approximate characteristics of the *stable condition of the polyhedral flame* structure is somewhat surprising. Why do the instability modes from the LSA correlate well with the experimentally observed cellular patterns which are stable and not constantly evolving? The following discussion addresses this aspect from multiple perspectives.

An important characteristic of the Bunsen flame is its confinement, caused by the flame anchoring at the burner rim. The cells are distributed along the circumference of the Bunsen flame, the number of cells is limited to integer values, and the cells arising in stable conditions are likely to be contracted or stretched to a small extent adjusting to the available space. If the burner circumference $D\pi$ is considered a characteristic hydrodynamic length scale confining the flame, an analogy can also be made with earlier studies on planar and circular flames.

Altantzis et al. [15] analyzed the instability developments of thermo-diffusively unstable planar H_2 flames and found that the number of cells, which form initially in the perturbed flame, can be roughly estimated based on the mode with the highest growth rate and the lateral domain size. This observation was independent of domain size, as shown in [15] for lateral sizes from 20 to $80\ell_T$. A similar study by Berger et al. [14] revealed that the fully developed lean H_2 flames tend to corrugate at a preferential wavelength, which coincides with the most unstable wavelength. This was also observed in domains with large lateral sizes. In contrast, for lateral sizes in the order of $\lambda(\omega_{max})$, which can be determined from the dispersion relation, the cell sizes appearing initially [15] and in the fully developed flames [14] are more dependent on domain size and are of the order of the critical wavelength λ_c, and can even be smaller than λ_c in the nonlinear regime [15]. In another work by Altantzis et al. [16] it was found that the range of rapidly growing wavelengths for perturbed circular expanding flames is comparable to the most unstable wavelength determined from the dispersion relation for planar flames.

The circumference of the burner used in this work is in the order of 110–$150\ell_T$ for the cases considered. Therefore, the development of the range of instability modes, including the most unstable ones, is not limited by this characteristic length scale of the flame. However, the important difference between planar and circular expanding flames compared to the Bunsen flame is the unconstrained development of large cell structures (higher wavelength modes) in the former. In the case of the Bunsen burner, the anchoring of the flame to the burner wall is one of the limiting factors for these higher wavelength modes. The development of larger cells would require a displacement of the flame from the anchoring location, i.e. the burner rim.

Further, an important limiting factor for cell formation are the associated time scales. Since the inverse of the growth rate $1/\omega$ corresponds to a time scale of the respective instability mode, the modes corresponding to (or close to) the highest growth rate have the shortest time scales. They will therefore develop the fastest and persist until other instability modes are formed. Thus, moving away from the most prominent mode of the dispersion relation to either side results in larger timescales for other modes. As observed in planar flames, cell structures larger than $\lambda(\omega_{max})$ take more time to develop and last longer, until they are split again into the smaller cells [12,15].

In Bunsen flame configurations, additional associated limiting time scales related to the burner geometry and inlet flow (convective time scales) can be analysed in relation to the instability time scales. Therefore, the time scales corresponding to the maximum growth rates from the dispersion relation are calculated and compared with the residence time, i.e. the time a fluid element needs to reach the flame tip (see Table 2). By multiplying the maximum growth rate and the introduced residence time, $\omega_{max} \cdot t_{res}$, one obtains a dimensionless parameter representing the ratio of the convective and the instability time scale $t_{inst} = 1/\omega_{max}$. Both

Please cite this article as: H. Lulic, A. Breicher, A. Scholtissek et al., On polyhedral structures of lean methane/hydrogen Bunsen flames: Combined experimental and numerical analysis, Proceedings of the Combustion Institute, https://doi.org/10.1016/j.proci.2022.07.251

these time scales are given in Table 2. Note that the corresponding ratio is determined only for the most unstable mode (ω_{max}), and the value corresponding to all other modes is lower.

For parameter values much higher than unity, there is enough time for the corresponding instability to grow remarkably, while the opposite is true for values much lower than unity. The estimated values here range from 5.7–16, with the lowest and highest values for the 50% H_2 − ϕ0.80 and 85% H_2 − ϕ0.65 cases, respectively. The time scales ratio can qualitatively describe the onset of instabilities observed in the experiment. The fact that they are of a similar order of magnitude can explain why the instabilities are sensitive to the inlet velocity, which can change the residence time, and the onset of instabilities can be shifted.

The similarity in time scales can further be indicative for the secondary cellular structures observed at the flame tip (see Fig. 1, right), where both intrinsic instability, differential diffusion and convection mechanisms play a role. Further investigations are required to characterise the secondary cellular structure in detail. In this case, local equivalence ratio and local mixture composition, which may differ from the initial mixture, play an essential role and different intrinsic length and time scales are to be expected for the local conditions close to the corrugated flame tip.

A relation of the presented results can also be drawn to the work of Sivashinsky [11] who performed linear stability analyses of planar and spherical/cylindrical flames using asymptotic theory for sub-critical Le_{eff} number mixtures. The theoretical dispersion relation for planar flames and the family of dispersion relations for spherical/cylindrical flames stabilised on a point source were compared, for different radii R. Different states from smooth, through regular stable cellular structure, to absolutely unstable flame propagation were found with increasing radii R and described accordingly with the shift of the dispersion relations in y (ω) direction as a function of R [11]. This shift implies narrowed range of the unstable modes around the $\lambda(\omega_{max})$, for lower values of radii R, and helps explain the possibility of the existence of a regular stable cellular structure also in case of Bunsen flames for a certain range of burner radii, where the most unstable modes are dominant.

5. Summary

In this work, characteristics of premixed CH_4 /H_2-air polyhedral Bunsen flames are systematically analyzed by means of a combined experimental and numerical study. The investigation includes mixtures with hydrogen contents varying from 20 to 85 Vol.-% and two equivalence ratios (0.8 and 0.65). The experiments are carried out with a laminar jet burner and encompass chemiluminescence imaging together with Planar Laser-induced Fluorescence measurements of the OH radical. The experiments are complemented by a linear stability analysis (LSA) of planar flames, whose initial conditions are comparable to the experiments.

The burner circumference $D\pi$ is the characteristic hydrodynamic length scale along which the cellular structures are distributed. It is found that the cell sizes at the base of the polyhedral Bunsen flames, which are determined from the experiments, decrease almost linearly with hydrogen addition and a weak dependence on the equivalence ratio is noted. It is further observed that the onset of instabilities is slightly affected by the equivalence ratio. The comparison of the length scales between experimental and numerical results reveals that the wavelength with the maximum growth rate predicted by the LSA is well correlated with the cell size obtained from the experiment. Notably, the overall decrease of the cell size and the strengthening of the cellular structure with hydrogen addition observed in the experiment is well captured by the numerical results. Furthermore, the cell size is only weakly affected by the equivalence ratio in the range from the experiment ($\phi = 0.8 - 0.65$) which is in agreement with the weak effect of the equivalence ratio on the maximum growth rate wavelength in the dispersion relations, while non-linear increase in the cell size is expected as lean limit is approached.

Overall, the systematic analysis shows that the intrinsic instabilities in planar flames can unravel the characteristics of the flame structure and quantify the instability length scales in polyhedral Bunsen flames reasonably well. Future work should address in more detail the time scales associated with the characteristic cellular patterns and the transition to secondary cellular structures observed at the flame tip for higher hydrogen contents.

Declaration of Competing Interest

The authors declare that they have no known competing financial interests or personal relationships that could have appeared to influence the work reported in this paper.

Acknowledgments

HL acknowledges funding by the Fritz and Margot Faudi-Foundation - Project No. 55200502. DG and AB were financially supported by the European Regional Development Fund (ERDF, project number: FPG991 0005/2019).

Supplementary material

Supplementary material associated with this article can be found, in the online version, at doi:10.1016/j.proci.2022.07.251.

Please cite this article as: H. Lulic, A. Breicher, A. Scholtissek et al., On polyhedral structures of lean methane/hydrogen Bunsen flames: Combined experimental and numerical analysis, Proceedings of the Combustion Institute, https://doi.org/10.1016/j.proci.2022.07.251

References

[1] M. Matalon, Intrinsic flame instabilities in premixed and nonpremixed combustion, Annu. Rev. Fluid Mech. 39 (2007) 163–191.
[2] F. Creta, P.E. Lapenna, R. Lamioni, N. Fogla, M. Matalon, Propagation of premixed flames in the presence of Darrieus–Landau and thermal diffusive instabilities, Combust. Flame 216 (2020) 256–270.
[3] M. Matalon, C. Cui, J.K. Bechtold, Hydrodynamic theory of premixed flames: effects of stoichiometry, variable transport coefficients and arbitrary reaction orders, J. Fluid Mech. 487 (2003) 179210.
[4] P.E. Lapenna, R. Lamioni, G. Troiani, F. Creta, Large scale effects in weakly turbulent premixed flames, Proc. Combust. Inst. 37 (2019) 1945–1952.
[5] G.H. Markstein, Nonsteady Flame Propagation, Pergamon Press, 1964.
[6] C.K. Law, Combustion Physics, Cambridge University Press, 2006.
[7] A. Smithells, H. Ingle, The structure and chemistry of flames, J. Chem. Soc. Trans. 61 (1892) 204–216.
[8] F.A. Smith, S.F. Pickering, Bunsen flames of unusual structure, Proc. Symp. Combust. 1–2 (1948) 24–26.
[9] S. Sohrab, C. Law, Influence of burner rim aerodynamics on polyhedral flames and flame stabilization, Combust. Flame 62 (1985) 243–254.
[10] A.N. Jacobi, S.H. Sohrab, Chemical kinetic and thermal aspects of cellular premixed flames, Combust. Sci. Technol. 69 (1990) 17–32.
[11] G. Sivashinsky, On self-turbulization of a laminar flame, Acta Astronaut. 6 (1979) 569–591.
[12] S. Kadowaki, H. Suzuki, H. Kobayashi, The unstable behavior of cellular premixed flames induced by intrinsic instability, Proc. Combust. Inst. 30 (2005) 169–176.
[13] S. Kadowaki, T. Hasegawa, Numerical simulation of dynamics of premixed flames: flame instability and vortex-flame interaction, Prog. Energy Combust. Sci. 31 (2005) 193–241.
[14] L. Berger, K. Kleinheinz, A. Attili, H. Pitsch, Characteristic patterns of thermodiffusively unstable premixed lean hydrogen flames, Proc. Combust. Inst. 37 (2019) 1879–1886.
[15] C. Altantzis, C.E. Frouzakis, A.G. Tomboulides, M. Matalon, K. Boulouchos, Hydrodynamic and thermodiffusive instability effects on the evolution of laminar planar lean premixed hydrogen flames, J. Fluid Mech. 700 (2012) 329361.
[16] C. Altantzis, C.E. Frouzakis, A.G. Tomboulides, K. Boulouchos, Direct numerical simulation of circular expanding premixed flames in a lean quiescent hydrogen-air mixture: phenomenology and detailed flame front analysis, Combust. Flame 162 (2015) 331–344.
[17] F. Creta, N. Fogla, M. Matalon, Turbulent propagation of premixed flames in the presence of Darrieus-Landau instability, Combust. Theory Model. 15 (2011) 267–298.
[18] C. Law, C. Sung, Structure, aerodynamics, and geometry of premixed flamelets, Prog. Energy Combust. Sci. 26 (2000) 459–505.
[19] Y. Mizobuchi, T. Takeno, A numerical study on the detailed structure of hydrogen/air bunsen flame, J. Combust. Soc. Japan 59 (2017) 303–311.
[20] A. Attili, R. Lamioni, L. Berger, K. Kleinheinz, P.E. Lapenna, H. Pitsch, F. Creta, The effect of pressure on the hydrodynamic stability limit of premixed flames, Proc. Combust. Inst. 38 (2021) 1973–1981.
[21] P.E. Lapenna, R. Lamioni, F. Creta, Subgrid modeling of intrinsic instabilities in premixed flame propagation, Proc. Combust. Inst. 38 (2021) 2001–2011.
[22] E. Al Sarraf, C. Almarcha, J. Quinard, B. Radisson, B. Denet, P. Garcia-Ybarra, Darrieus-Landau instability and markstein numbers of premixed flames in a hele-shaw cell, Proc. Combust. Inst. 37 (2) (2019) 1783–1789.
[23] M. Tayyab, B. Radisson, C. Almarcha, B. Denet, P. Boivin, Experimental and numerical Lattice-Boltzmann investigation of the Darrieus–Landau instability, Combust. Flame 221 (2020) 103–109.
[24] G. Troiani, F. Creta, M. Matalon, Experimental investigation of Darrieus-Landau instability effects on turbulent premixed flames, Proc. Combust. Inst. 35 (2) (2015) 1451–1459.
[25] F. Creta, R. Lamioni, P.E. Lapenna, G. Troiani, Interplay of Darrieus-Landau instability and weak turbulence in premixed flame propagation, Phys. Rev. E 94 (2016) 053102.
[26] R. Rasool, N. Chakraborty, M. Klein, Effect of non-ambient pressure conditions and lewis number variation on direct numerical simulation of turbulent bunsen flames at low turbulence intensity, Combust. Flame 231 (2021) 111500.
[27] H.G. Weller, G. Tabor, H. Jasak, C. Fureby, A tensorial approach to computational continuum mechanics using object-oriented techniques, Comput. Phys. 12 (1998) 620–631.
[28] A. Stagni, A. Frassoldati, A. Cuoci, T. Faravelli, E. Ranzi, Skeletal mechanism reduction through species-targeted sensitivity analysis, Combust. Flame 163 (2016) 382–393.
[29] J.O. Hirschfelder, C.F. Curtiss, R.B. Bird, Molecular Theory of Gases and Liquids, second ed., John Wiley and Sons, Inc., New York, 1964.
[30] A. Ern, V. Giovangigli, Multicomponent Transport Algorithms, Springer Berlin Heidelberg, 1994.
[31] T. Howarth, A. Aspden, An empirical characteristic scaling model for freely-propagating lean premixed hydrogen flames, Combust. Flame 237 (2022) 111805.
[32] J. Yu, R. Yu, X. Bai, M. Sun, J. Tan, Nonlinear evolution of 2D cellular lean hydrogen/air premixed flames with varying initial perturbations in the elevated pressure environment, Int. J. Hydrog. Energy 42 (6) (2017) 3790–3803.
[33] G. Sivashinsky, Diffusional-thermal theory of cellular flames, Combust. Sci. Technol. 15 (1977) 137–145.

Please cite this article as: H. Lulic, A. Breicher, A. Scholtissek et al., On polyhedral structures of lean methane/hydrogen Bunsen flames: Combined experimental and numerical analysis, Proceedings of the Combustion Institute, https://doi.org/10.1016/j.proci.2022.07.251